NUCL SCI TECH (2019) 30:53
https://doi.org/10.1007/s41365-019-0576-4

Performance of an electron linear accelerator for the first photoneutron source in China

Xuan Li[1,2,3] · Jun-Qiang Zhang[1,2] · Guo-Qiang Lin[1,2] · Wen-Cheng Fang[1,2] · Qiang Gu[1,2] · Meng Zhang[1,2]

Received: 30 August 2018 / Revised: 25 October 2018 / Accepted: 31 October 2018 / Published online: 7 March 2019

Abstract A compact 15.0-MeV, 1.5-kW electron linear accelerator (LINAC) was successfully constructed to provide an electron beam for the first photoneutron source at the Shanghai Institute of Applied Physics, Shanghai, China. This LINAC consists of five main parts: a thermal cathode grid-controlled electron gun, a pre-buncher, a variable-phase-velocity buncher, a light-speed accelerating structure, and a high-power transportation beamline. A digital feedforward radio frequency compensator is adopted to reduce the energy spread caused by the transient beam loading effect. Furthermore, a real-time electron gun emission feedback algorithm is used to keep the beam stable. After months of efforts, all the beam parameters successfully met the requirements of the facility. In this paper, the beam commissioning process and performance of the LINAC are presented.

Keywords Electron linear accelerator · High-power transportation beamline · Digital feedforward radio frequency compensation · Real-time electron gun emission feedback algorithm · Transmission efficiency

This work was supported by the Youth Innovation Promotion Association CAS (No. 2018300).

✉ Meng Zhang
zhangmeng@sinap.ac.cn

1 Shanghai Institute of Applied Physics, Chinese Academy of Sciences, Shanghai 201800, China

2 Shanghai Synchrotron Radiation Facility, Chinese Academy of Sciences, Shanghai 201204, China

3 University of Chinese Academy of Sciences, Beijing 100049, China

1 Introduction

The energies of neutrons produced in a target bombarded by pulses of high-energy electrons from a linear accelerator (LINAC) may be determined with high resolution by employing time-of-flight techniques [1–4]. A photoneutron source (PNS) with appropriate parameters is a powerful tool for producing intense pulsed neutron beams. As an auxiliary project of the Thorium Molten Salt Reactor Energy System (TMSR) program at the Shanghai Institute of Applied Physics (SINAP) in Shanghai, China, in the first stage, the application of the PNS focuses on thermal neutron data measurement with a relatively lower neutron flux [2], and hence, the facility employs a 15 MeV electron LINAC, bombarding a tungsten target with 1.5 kW electrons to produce neutrons. In the future, with the requirement for higher fast neutron flux [2], the LINAC beam energy will be upgraded to 100 MeV for the final stage and at this bombarding target energy of the beam, the neutron yield will almost saturate [5]. Presently, we have successfully completed this first stage work, including the technical design, assembly, radio frequency (RF) and high voltage (HV) conditioning, and beam commissioning of the machine. A schematic drawing of the PNS is shown in Fig. 1. The whole PNS is composed of four main areas: the neutron experimental area, the LINAC, power source cabinets, and a control area. The results of beam acceleration testing as well as an overview of the whole LINAC system will be presented in this paper.

1.1 Overview of the LINAC

The 15-MeV, 1.5-kW LINAC consists of a thermal cathode grid-controlled electron gun (E-Gun), a standing-

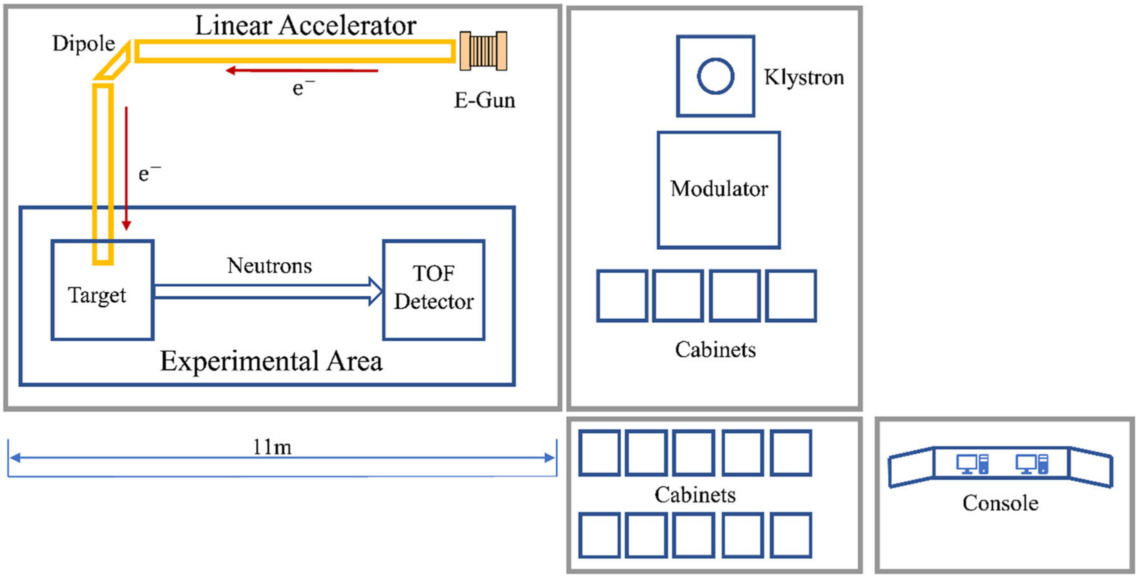

Fig. 1 Layout (plan view) of the PNS (phase-I)

wave pre-buncher, a traveling-wave buncher (TWB), and a light-speed accelerating structure. After the beam travels through the LINAC, highly efficient beam collimation and transportation can be achieved in a high-power transportation beamline (HPTB) [6]. Figure 2 gives the layout of the whole LINAC for the PNS (phase-I) facility.

A thermal cathode grid-controlled E-Gun is employed as the electron source [7, 8]. The voltage between the anode (grounded) and the cathode is − 60 kV. The cathode grid assembly is a Y646B from Eimac CPI, which can meet the requirement of a maximum beam current of 1 A. One amplifier, which is designed by SINAP, is adopted to drive the cathode with a 0.5–3.0 μs pulse width. An HV direct current (DC) power supply (model WR125N2 from Glassman) is adopted to provide − 60 kV voltage between the anode and the cathode.

To increase the efficiency of beam capture and acceleration, a bunching system consisting of a pre-buncher and

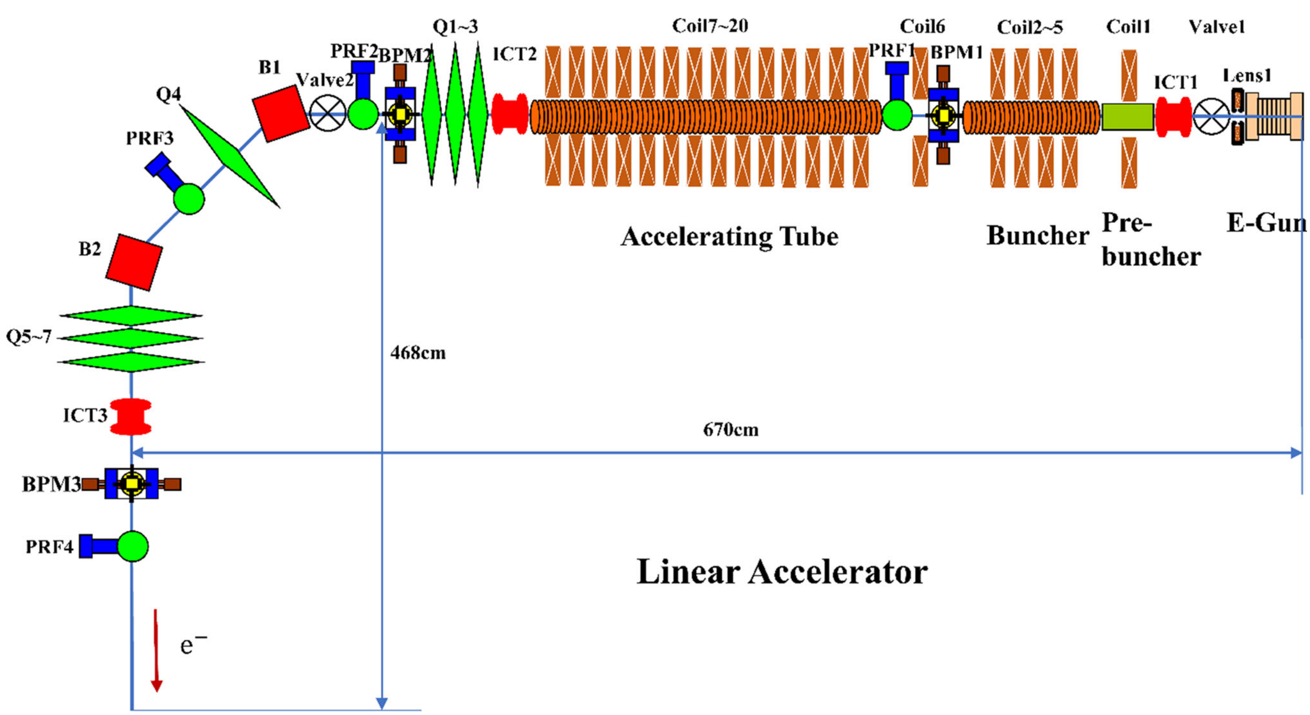

Fig. 2 (Color online) Layout of the LINAC for the PNS (phase-I)

a buncher in sequence is employed immediately following the E-Gun.

For the cavity of the pre-buncher, we employ a conventional reentrant type structure. This cavity is a standing-wave cavity made of stainless steel with a nickel-coated surface inside. The major design parameters of the pre-buncher cavity are listed in Table 1. A particular solid amplifier of maximum power of 4.0 kW is adopted to provide the RF power to the pre-buncher [9].

After traveling through the pre-buncher, the beam will be bunched and accelerated further by a multiple-cell disk-load TWB, which works in the $2\pi/3$ mode. This TWB consists of 16 disk-load cells including the input and the output coupler cavities. To improve the capture efficiency, before the light-speed cells, the characteristic parameters of the first six cells vary slightly and the other ten cells comprise the constant-phase-velocity constant-impedance structure. The cells' main design parameters and geometry dimensions are listed in Tables 2 and 3, respectively. In Table 3, β_p is the normalized phase velocity of the accelerating cell, β_g is the normalized group velocity of the accelerating cell, t_f is the filling time of the accelerating cell, α is the attenuation constant per unit length, Q is the quality factor of the accelerating cell, R_m is the shunt impedance per unit length, and f is the working frequency of the accelerating cell.

Figure 3 gives the structure schematic of the disk-loaded or iris-loaded waveguide [10–14]. This bunching scheme had already been successfully proved to be practicable and efficient on an industrial LINAC with 1 kW (2 MeV) averaged beam power at SINAP. In addition, to avoid beam losses transversely, the conventional focusing method of solenoid coils is employed to provide the focusing force.

After the two bunching sections, a light-speed accelerating structure is employed to accelerate the beam from 2 MeV to the designed beam energy of 15 MeV. For the light-speed section, there are two kinds of structures. After investigation, including considerations of cost and efficiency, the decision was made to employ a constant-impedance disk-load accelerating structure for our LINAC. It is also a traveling-wave structure that works in the $2\pi/3$ mode, Tables 4 and 5 give the major design parameters and dimensions of the accelerating tube. In Table 5, β_p is the normalized phase velocity of the accelerating cell, α is the attenuation constant per unit length, a is the radius of the aperture, b is the radius of the waveguide, Q is the quality factor of the accelerating cell, R_m is the shunt impedance per unit length, and f is the working frequency of the accelerating cell.

The input RF high power for the buncher and the accelerating tube is generated simultaneously by the two-stage amplifiers. In the first stage, a solid-state amplifier having a maximum output power of 1.0 kW is employed to amplify the 0–5 dBm signal from the low-level radio frequency (LLRF). The final-stage amplifier, equipped with a Toshiba E37308 klystron, provides the maximum output of 27.5 MW.

The power attenuation of the standard rectangular waveguide BJ32 is 0.46% per meter. The distance from the klystron to the buncher and the accelerating tube is ~ 10 m, so given the power loss of the flanges and ceramic windows; the total loss of the RF transportation line is estimated to be 10%. With the total input power of 16.4 MW to the buncher and accelerating tube, the output RF power of the klystron should be at least 18.3 MW, which is available from the power source. There is a 9-dB power divider between the buncher and the accelerating tube; through it, 2 MW of RF power is fed into the buncher. The remaining 14.4 MW of power is offered to the accelerating tube. The high-power phase shifter between the buncher and the accelerating tube can be used to control the RF phase separately for the two sections.

Table 1 Main design parameters of the pre-buncher

Parameter	Value
Operating frequency (MHz)	2856
Gap voltage (kV)	~ 25 (adjustable)
Q factor	963
Total length (mm)	342.76
Drift length (mm)	176.38
Cavity length (mm)	30.6
Gap length (mm)	8.89
Beam aperture (mm)	19.05
Power capacity (kW)	2.0
Coupling coefficient	1.04

Table 2 Major design parameters of the TW buncher

Parameter	Value
Operating frequency (MHz)	2856
Working mode	$2\pi/3$
Cell number	16
Total length (m)	0.57
Voltage standing-wave ratio (VSWR)	< 1.1
Bandwidth (VSWR = 1.2) (MHz)	4
Phase advance per period (°)	120 ± 2.5
Working temperature (°C)	45 ± 0.1
Input RF power (MW)	2
Output electron energy (MeV)	2

Table 3 Cell parameters and dimensions of the TW buncher

Cell no.	β_p	β_g (%)	t_f (ns)	α	a (mm)	b (mm)	Q	R_m (MΩ/m)	f (MHz)
1	0.63	0.7167	1.02594E−08	0.4507	10	41.502	9266	25.757	2856.035
2	0.6	0.7068	1.04031E−08	0.4801	10	41.575	8820	22.834	2856.005
3	0.6	0.7068	1.04031E−08	0.4801	10	41.575	8820	22.834	2856.005
4	0.87	0.7455	9.8631E−09	0.3258	10	41.102	12,321.3	49.307	2856.006
5	0.93	0.7458	9.85913E−09	0.3094	10	41.035	12,968.3	54.926	2856.013
6	0.96	0.7456	9.86178E−09	0.3023	10	41.005	13,277.2	57.67	2856.002
7–16	0.98	0.7452	9.86707E−09	0.298	10	40.986	13,478	59.474	2856.001

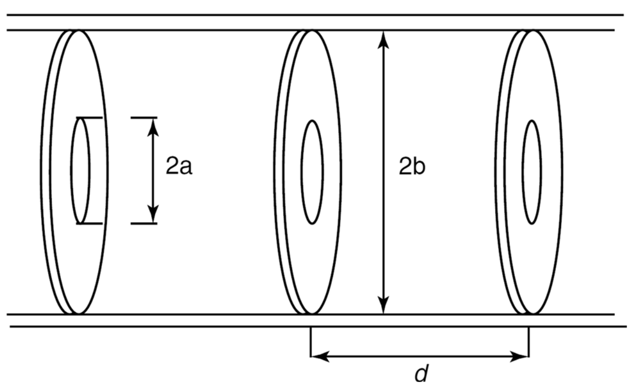

Fig. 3 Disk (iris)-loaded traveling-wave structure. 2a is the diameter of the aperture, 2b is the diameter of the waveguide, and d is the periodic length

Table 4 Major design parameters of the TW accelerating tube

Parameter	Value
Operating frequency (MHz)	2856
Working mode	$2\pi/3$
Cell number	40
Total length (m)	1.5
Shunt impedance (MΩ/m)	53
Total attenuation	0.24
Group velocity (v_g/c)	0.01546
VSWR	< 1.1
Bandwidth (VSWR = 1.2) (MHz)	4
Phase advance per period (°)	120 ± 2.5
Working temperature (°C)	45 ± 0.1
Input RF power (MW)	14
Output electron energy (MeV)	14.4

After the accelerating tube, to transport the 15-MeV, 1.5-kW beam to the target area efficiently (see Fig. 1), a well-designed HPTB is established. At the beginning of the HPTB, an integrating current transformer (ICT2), a beam position monitor (BPM2), and a profile (PRF2) are sequentially installed to calibrate the beam quality before it travels through the dipoles. The quadrupole triplet of Q1–Q3 is used to match the beam transverse envelope when the beam travels through the two 45-degree dipoles. Dipole B1, quadrupole Q4, and dipole B2 comprise a typical achromatic lattice to optimize the transmission efficiency between the two dipoles. The quadrupole triplet of Q5–Q7 is designed to match the envelope and the beam size on the tungsten target in the experimental zone. With ICT3, BPM3, and PRF4, we can get the beam performance after transportation. Based on the above configuration, a transmission of nearly 90% is reached.

2 Commissioning and testing

Beam commissioning and beam acceleration testing of the LINAC are performed in the following three steps:

The first step is to perform RF power conditioning in the rectangular waveguide BJ32, the high-power phase shifter, the buncher, and the accelerating tube. Meanwhile, HV conditioning and cathode activation of the E-Gun are also performed. During this stage, because vacuum sparking and outgassing occur very frequently, it is indispensable to change the machine protection system from the beam commissioning mode to the RF conditioning mode. After approximately 1 week of conditioning time spent for the RF components mentioned above, the LINAC worked

Table 5 Cell parameters and dimensions of the TW accelerating tube

Cell no.	β_p	α	a (mm)	b (mm)	Q	R_m (MΩ/m)	f (MHz)
1–40	1	0.1411	12.115	41.475	13,717	53.22	2856.001

successfully with a modulator HV of 33 kV, an E-Gun HV of $-$ 60 kV, and a filament readback voltage of $>$ 6.0 V [15].

After finishing step one above, the electron beam commissioning commenced. Because of the $>$ 20-W beam power of every 3 μs length pulse for the nominal working mode, it is safer and more practical to perform beam commissioning with a rather shorter pulse such as $\sim$ 3 ns and a lower repetition frequency such as 1 Hz. In that mode, we can adjust the configurations of solenoids, lenses, correctors, phases, and power amplitudes to get a suitable beam size on the screens of PRF1–PRF4 and ICT1–ICT3. The beam acceleration in the RF structures and beam optics transportation along the whole accelerator were optimized successfully [16, 17].

The last key step is to increase the average power gradually by increasing the pulse length and repetition frequency sequentially. First, we gradually increased the length of the pulse to 3 μs. During this process, special attention had to be paid to the transient beam loading effect [10], which can cause a rather large energy spread. Because of the limited beam pipe aperture, it would decrease the transmission efficiency of the beam when it traveled through the two 45-degree dipoles. Moreover, such a high beam power bombarding the beam pipe poses a danger to the chamber. It would probably melt the vacuum chamber and lead to air leakage. Another problem is the radiation protection corresponding to the beam loss. Therefore, a digital feedforward RF compensator, which uses a digital LLRF feedforward method to compensate for the RF power output, was successfully developed to decrease the energy spread caused by the transient beam loading effect [18–21].

After the LINAC configuration of the 3 μs pulse length is finished, the repetition frequency of the whole LINAC will be increased. During this process, with the increase in the beam power and temperature corresponding to the beam bombarding onto the surface of the tungsten target, the vacuum condition deteriorated seriously and quickly. It took a relatively long time for us to solve this problem.

Because of space limitations, just after the exit of the accelerating tube, we employed an HPTB including two 45-degree dipoles to transport the 1.5 kV beam to the target area. There are both advantages and challenges with this design. Like the function of a real-time, online energy analysis station, the HPTB ensures that the beam quality of every pulse provided for the PNS is good enough and reproductive. Meanwhile, we should also make sure that the LINAC has higher stability and safety. For rather heavy beam loading, without changing the input RF power, the current of the beam should be stable enough to avoid beam loss in the HPTB section. However, the beam current will decrease slowly as the operating time increases or the repetition frequency increases. This might possibly be attributed to the "cooling" of the cathode, because the more thermionic electrons that are emitted, the more heat will be taken from the cathode. Therefore, we developed a real-time E-Gun emission feedback algorithm to keep the emitted beam current constant by changing the filament current setting value of the E-Gun in steps of 1 mA in real time.

Even with the algorithm deployed, several serious vacuum leakage events occurred, one of which led to breakage of the observing glass window of PRF4, perhaps because it had been somewhat compromised from radiation damage. Another main event was that the vacuum bellow close to the tungsten target was broken by high-power beam bombardment. We improved the vacuum bellow by adding a stainless-steel lining inside and solved this problem successfully.

After solving the above problems, about 6 months later, in January 2018, we passed the accelerator performance experts' test successfully. Table 6 gives the main measured parameters of the LINAC. At a repetition rate of 70 Hz, we reached $>$ 1.5 kW of average power.

The transmission efficiency is another main parameter with which we are concerned. After a careful beam commissioning and long-time operating test, the transmission efficiency of the HPTB reached $\sim$ 90%, as shown in Fig. 4 (and calculated by Area(3) $\times$ 2/Area(2) = 88.8%); this is consistent with the design value.

If the input RF power is constant, because of the beam loading effect, changing the injected beam current would affect the energy at the exit of the LINAC. A study of the characteristics of the relationship between the energy and the injected beam current was conducted, and the results indicate that the measurements agree well with the analytical results, as shown in Fig. 5.

The power remaining through the output coupler of the accelerating tube can be calibrated by the LLRF too [22]. As the beam current increases, the RF power remaining decreases from 3.8 to 1.8 MW. The relation is shown in Fig. 6, and the measured values are fairly well reproduced by the calculated values. Comparing Fig. 5 with Fig. 6, we can see the obvious beam loading effect on a high average beam power LINAC.

Table 6 Beam parameters of performance testing for the 15-MeV, 1.5-kW LINAC

Parameter	Measured	Designed
Energy (MeV)	16.6	$\geq$ 15
Power on the tungsten target (W)	1558.37	$\geq$ 1500
Stability of the beam current	0.37%/30 min	$\leq$ 1%/30 min
Pulse width (μs)	2.83	0.5–3.0

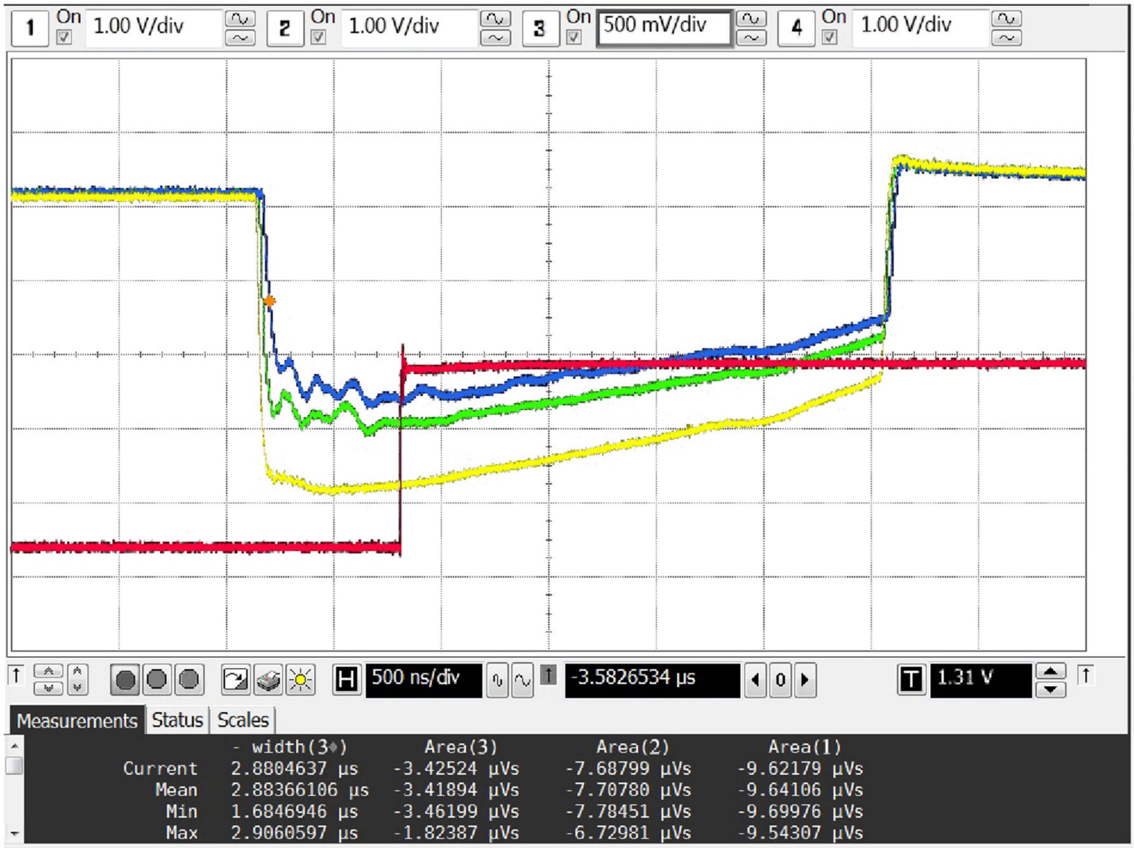

Fig. 4 (Color online) Transmission efficiency of the LINAC. The green and blue lines indicate the signals acquired from ICT2 and ICT3, respectively. The two columns named Area(2) and Area(3) in the bottom show the charge values processed by the oscilloscope

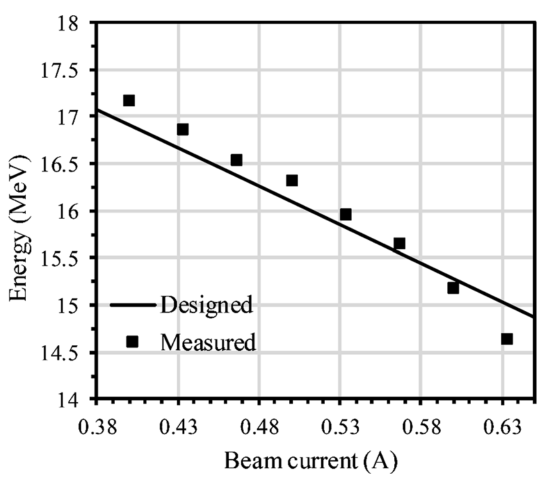

Fig. 5 Final energy as a function of the injected beam current

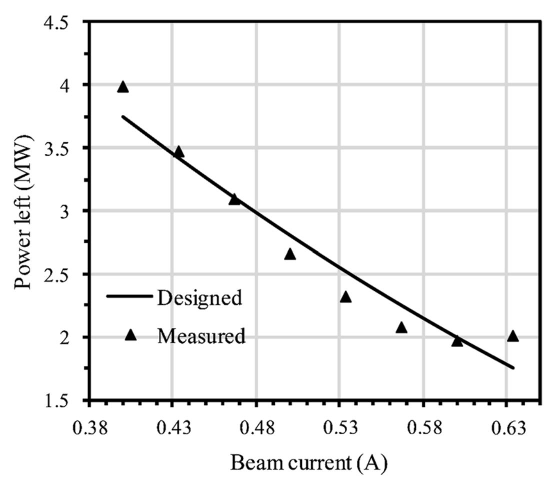

Fig. 6 RF power remaining as a function of the injected beam current

3 Conclusion

An electron LINAC with an energy of 15 MeV and an average power of 1.5 kW was designed and constructed successfully for the first photoneutron source (PNS phase-I) in China. It consists of an E-Gun, a pre-buncher, a buncher, an accelerating structure, and an HPTB. It took about 6 months to perform the RF and HV conditioning and beam commissioning. To meet those challenges corresponding to the HPTB, several measures were developed, including use of a digital feedforward RF compensator, design of a real-time E-Gun emission feedback algorithm, and deployment of a stainless-steel lining inside the vacuum bellow. According to the measured values, these measures worked well and solved the problems. The beam parameter tests were performed, and the measured results indicated good performance of the electron LINAC.

The completion and success of the first stage of the LINAC give us valuable experience regarding beam commissioning and several useful developed measures, which will be indispensable for the LINAC upgrade with higher beam energy and higher beam power. These efforts will also build a firm foundation for starting the PNS project of TMSR.

Acknowledgements We would like to express our sincere thanks to SINAP members of the Department of Reactor Physics. We are also very grateful to the SINAP members of the Vacuum Group, Power Supply Group, Beam Instrumentation Group, Control Group, and Pulse Group for technical assistance.

References

1. Z.K. Lin, G.M. Sun, J.G. Chen et al., Simulation and optimization for a 30-MeV electron accelerator driven neutron source. Nucl. Sci. Tech. **23**, 272–276 (2012). https://doi.org/10.13538/j.1001-8042/nst.23.272-276
2. L.X. Liu, H.W. Wang, Y.G. Ma et al., Measurements of the total cross section of natBe with thermal neutrons from a photo-neutron source. Nucl. Instrum. Meth. B **410**, 158–163 (2017). https://doi.org/10.1016/j.nimb.2017.08.022
3. H.W. Wang, J.G. Chen, X.Z. Cai et al., Development of photo-neutron facility driven by electron LINAC. Nucl. Tech. **37**, 100522 (2014). https://doi.org/10.11889/j.0253-3219.2014.hjs.37.100522. **(in Chinese)**
4. R.M. Ji, M.H. Li, Y. Zou et al., Impact of photoneutrons on reactivity measurements for TMSR-SF1. Nucl. Sci. Tech. **28**, 76 (2017). https://doi.org/10.1007/s41365-017-0234-7
5. W.P. Swanso, *Radiological Safety Aspects of the Operation of Electron Linear Accelerators* (IAEA, Vienna, 1979), pp. 79–96
6. M. Zhang, X. Li, W.C. Fang et al, Linac design for nuclear data measurement facility, in *Proceedings of Proceedings of the 4th International Particle Accelerator Conference (IPAC)*, Shanghai, China, May 2013, pp. 1229-1231
7. Z. Nergiz, A. Aksoy, Injector of the Turkish light source facility TURKAY. Nucl. Sci. Tech. **28**, 161 (2017). https://doi.org/10.1007/s41365-017-0306-8
8. B.C. Jiang, G.Q. Lin, B.L. Wang et al., Multi-bunch injection for SSRF storage ring. Nucl. Sci. Tech. **26**, 050101 (2015). https://doi.org/10.13538/j.1001-8042/nst.26.050101
9. H.L. Ding, M.H. Zhao, C.C. Xiao et al., An S-band solid-state radio frequency power amplifier used at Shanghai soft X-ray FEL facility. Nucl. Sci. Tech. **27**, 146 (2016). https://doi.org/10.1007/s41365-016-0144-0
10. T.P. Wangler, *RF Linear Accelerators*, 2nd edn. (Wiley-VCH, Weinheim, 2008)
11. R.B. Neal, *The Stanford Two Mile Accelerator* (W.A. Benjamin, Inc., New York, 1968)
12. J.H. Tan, D.C. Tong, Q. Gu et al., Development of a nonresonant perturbation technique and its application to multicell traveling-wave deflectors. Nucl. Instrum. Meth. A **835**, 148–156 (2016). https://doi.org/10.1016/j.nima.2016.08.039
13. Z.T. Zhao, C. Feng, K.Q. Zhang et al., Two-stage EEHG for coherent hard X-ray generation based on a superconducting linac. Nucl. Sci. Tech. **28**, 117 (2017). https://doi.org/10.1007/s41365-017-0258-z
14. C. Feng, H.X. Deng, Review of fully coherent free-electron lasers. Nucl. Sci. Tech. **29**, 160 (2017). https://doi.org/10.1007/s41365-018-0490-1
15. Eimac, CPI, Electron Sources(2018). www.cpii.com/product.cfm/9/22/131. Accessed 29 Aug. 2018
16. W.Y. Zhang, X.Q. Liu, L. Feng et al., 2856 GHz microwave signal extraction from mode-locked Er-fiber lasers with sub-100 femtosecond timing jitter. Nucl. Sci. Tech. **29**, 91 (2018). https://doi.org/10.1007/s41365-018-0419-8
17. Q.L. Yu, D. Gu, M. Zhang et al., Transverse phase space reconstruction study in Shanghai soft X-ray FEL facility. Nucl. Sci. Tech. **29**, 9 (2018). https://doi.org/10.1007/s41365-017-0338-0
18. J.Q. Zhang, Y.J. Liu, S.P. Zhong et al., Low level radio frequency system of 15-MeV electrons linac. Nucl. Tech. **39**, 030403 (2016). https://doi.org/10.11889/j.0253-3219.2016.hjs.39.030403. **(in Chinese)**
19. S. Li, J.Q. Zhang, M. Zhang et al., Implementation of FPGA-based feedforward function in LLRF system for electron LINAC. Nucl. Tech. **39**, 070402 (2016). https://doi.org/10.11889/j.0253-3219.2016.hjs.39.070402. **(in Chinese)**
20. C.H. Miao, M. Liu, C.X. Yin et al., Precise magnetic field control of the scanning magnets for the APTRON beam delivery system. Nucl. Sci. Tech. **28**, 172 (2017). https://doi.org/10.1007/s41365-017-0324-6
21. X.H. Tang, Y.J. Liu, J.Q. Zhang et al., An automatic frequency control system based on MicroTCA. Nucl. Tech. **39**, 070102 (2016). https://doi.org/10.11889/j.0253-3219.2016.hjs.39.070102. **(in Chinese)**
22. Z.Q. Geng, Beam-based optimization of SwissFEL low-level RF system. Nucl. Sci. Tech. **29**, 128 (2018). https://doi.org/10.1007/s41365-018-0460-7